buildings

MDPI

Article

Full-Scale Test and Finite Element Analysis of Flat Tempered Glass Sheets Subjected to Long-Edge Bending

Wentao Li [1], Jie Ming [2], Wenjian Chen [1], Jianghao Zhou [3], Xiaoxiong Zha [1,*], Hualin Cao [3] and Wei Wei [3]

[1] School of Materials Science and Engineering, Harbin Institute of Technology, Shenzhen, Shenzhen 518055, China; liwentao2014@126.com (W.L.); 23s154054@stu.hit.edu.cn (W.C.)
[2] Shenzhen Bay Area Urban Construction and Development Co., Ltd., Shenzhen 518063, China; mj@szba-ucd.com.cn
[3] China Construction Buer Curtain Wall & Decoration Co., Ltd., Shenzhen 518052, China; q18620516390@163.com (J.Z.); caohualin1025@163.com (H.C.); weizhaowei2009@163.com (W.W.)
* Correspondence: zhaxx@hit.edu.cn

Abstract

Flat tempered glass sheets subjected to cold bending have been increasingly used in modern architectural curtain walls due to its extremely low production and processing costs and construction flexibility. However, existing studies mainly focus on small-size specimens, and there is still a lack of systematic understanding of the mechanical behavior of large-size monolithic tempered glass under long-edge cold bending. This knowledge gap leads to either unsafe or overly conservative curtain wall designs, limiting the popularization and application of flat tempered glass subjected to cold bending in large-curved curtain walls. This paper presents a comprehensive investigation into the bending behavior of flat tempered glass sheets—3200 mm × 1700 mm × 8 mm monolithic tempered glass—under long-edge cold bending conditions, through full-scale tests, finite element simulations and theoretical derivations. Firstly, cold bending tests on three full-scale tempered glass specimens were completed to obtain the failure process, failure modes, ultimate loads, failure displacements and stress distribution laws. The initial tempered residual stress of each specimen was measured to consider its influence on the mechanical response. Secondly, a refined finite element model was established in ABAQUS, which incorporated the initial tempered stress field, self-weight deformation and contact nonlinear effects. The accuracy of the model was verified through failure location, ultimate load, displacement and load-displacement curves, with average errors of less than 5.1% for both load and displacement predictions. Finally, parametric analysis was carried out based on the validated model to reveal the influence laws of glass width and thickness on the cold bending performance. The results show that glass thickness has the most significant influence on the bearing capacity, followed by length, while width has a relatively minor effect. This study provides basic data and model support for the safe application of flat tempered glass sheets subjected to long-edge bending.

Keywords: monolithic tempered glass; long-edge bending of tempered glass sheets; full-scale test; finite element analysis; parametric analysis; curtain wall engineering

Check for updates

Academic Editor: Vipul Patel

Received: 8 June 2026
Revised: 26 August 2026
Accepted: 4 September 2026
Published: 20 September 2026

Copyright: © 2026 by the authors. Licensee MDPI, Basel, Switzerland. This article is an open access article distributed under the terms and conditions of the Creative Commons Attribution (CC BY) license.

1. Introduction

With the continuous development of architectural design concepts and digital construction technologies, the facades of modern buildings are gradually evolving from traditional planar forms to free-form surfaces and complex hyperboloid forms. In response to this

development trend, Yang Rong earlier pointed out from the perspective of engineering application that cold bending technology can replace the hot bending process within a certain curvature range to realize the economical construction of curved glass curtain walls [1]. Fan Yuebo [2] further illustrated, combined with a natatorium project, that bidirectional curved surface effects can be achieved by flat plate cold bending through controlling the warping value of panels and optimizing the three-dimensional model. Sun Jian and Jin Zhiqiang took the daylighting roof project of Suzhou Center as the object, verified the feasibility of frame-supported flat tempered glass subjected to cold bending in special-shaped roofs, and further analyzed its long-term performance through fatigue tests [3]. Huang Jie [4] proposed from the perspective of integrated unit panel design and construction that cold-bent curtain wall design should integrate BIM lofting, finite element analysis and on-site verification to improve the consistency of panel design and installation. Li Shuailing et al. [5] carried out cold bending tests and finite element analysis on the glass curtain wall of the Oujia Building, indicating that cold bending technology has begun to be applied to ultra-complex hyperbolic glass curtain wall projects.

In engineering practice, Eekhout [6] showed through the case of the flat tempered glass subjected to cold bending roof of the Victoria and Albert Museum in London that flat tempered glass subjected to cold bending has been able to be used in representative complex public building skin systems. Focusing on the parametric design of flat tempered glass subjected to cold bending skins, existing studies have directly introduced computational design methods into the geometric generation and the panel partitioning process of glass curtain walls, thereby improving the constructability of free-form facades [7]. The research of Laurs and Feldmann [8] further pointed out that flat tempered glass subjected to cold bending design needs to form an independent technical path different from traditional flat glass analysis. In addition, studies on free-form curtain wall engineering have shown that the problem of flat tempered glass subjected to cold bending is essentially a comprehensive problem of the synergy of geometry, structure, manufacturing and installation, rather than a simple mechanical analysis problem [9].

In the basic mechanical research of flat tempered glass subjected to cold bending, Jiang Jialin [10] carried out a relatively systematic experimental study on the unidirectional cold bending of insulating tempered glass panels. Through orthogonal tests, distributed optical fiber monitoring and finite element analysis, he investigated the influences of cold bending radius, glass thickness and cavity thickness on the cold bending internal stress and sealing material deformation of insulating tempered glass panels, and proposed corresponding cold bending stress coefficients and deflection coefficients. Li Jiawen [11] further extended the research object to insulating laminated glass panels, pointing out that cold bending radius, single sheet thickness, cavity thickness and interlayer thickness all significantly affect the principal tensile stress, central deflection and interlayer relative slip, among which cold bending radius is still the most important control parameter. The research of Zhang Xide, Luo Di, Li Jiawen and Long Yanjie [12] on the mechanical response of unidirectional cold-bent insulating laminated glass panels showed that the synergy of the insulating layer and the interlayer significantly changes the stress and displacement distribution of the glass panel. Xu Zilin et al. [13] measured the stress distribution of cold-bent insulating glass panels using distributed optical fiber technology, verifying the applicability of the optical fiber method in the strain field identification of flat tempered glass subjected to cold bending. Jin Xiang [14] studied the forward mechanical performance and design method of cold-bent twisted laminated glass panels from the perspective of laminated glass, pointing out that interlayer materials, twist rate and glass thickness jointly affect the bearing capacity and deformation performance of components.

Compared with unidirectional cold bending, corner cold bending and bidirectional cold bending have more complex boundary conditions and more diverse deformation paths. Existing studies have experimentally analyzed the mechanical response and load coupling effect of laminated tempered glass under single-corner cold bending conditions, indicating that corner displacement significantly changes the in-plane stress path and deformation mode [15]. In the selection of complex curved curtain wall schemes, some studies have compared single-corner cold bending and free-form cold bending schemes, emphasizing that differentiated panel implementation paths should be adopted under different geometric conditions [16]. Rahimzadeh et al. [17] further introduced machine learning methods into extreme cold bending geometry prediction, indicating that cold bending research has gradually expanded from traditional mechanical analysis to integrated prediction of form-structure-manufacturing. The research of Zhang Xide et al. [18] on the negative coupling bearing performance of hyperbolic cold-bent tempered glass panels pointed out that there is a significant coupling effect between cold bending residual stress and external loads, and the cold bending method directly affects the ultimate bearing state of the glass panel.

Wang Wanning et al. [18] discussed the strength safety judgment problem of curved laminated insulating glass under cold bending forming conditions from the perspective of engineering design, pointing out that cold bending load, temperature effect, interlayer shear and load holding time jointly determine the safety state of glass. On this basis, relevant studies further proposed a simplified calculation method for glass stress considering cold bending effect, and verified through plate and shell theory and finite element that cold bending stress has a strong correlation with curvature change [19]. Aiming at engineering implementation problems, Sun Jian and Jin Zhiqiang [20] also summarized the construction technology and checking method of frame-supported flat tempered glass subjected to cold bending from the perspective of reliability research.

Focusing on the inherent response of flat tempered glass subjected to cold bending, existing studies have investigated the stress and deformation development laws of monolithic glass during cold bending forming, indicating that the cold bending process itself can lead to a significant non-uniform stress state on the plate surface [21]. Laurs et al. [22] studied the inherent stress state of flat tempered glass subjected to cold bending through experiments and numerical analysis, providing a basis for subsequent model establishment. Galuppi and Riva [23] experimentally and numerically characterized the torsional cold bending response of thin glass, revealing the mechanical characteristics of torsional cold-bent plates under nonlinear conditions. In terms of insulating glass, existing studies have analyzed the mechanical response of complex double-plate systems starting from anticlastic cold-bent insulating glass and its coupling effect with uniform load [24]; meanwhile, studies on the mechanical behavior of cold-bent insulating glass units have shown that the air layer and edge structure have a significant impact on the cooperative work of the two plates [25]. Van Driel et al. [26] further studied the cold bending behavior of double insulating glass units with rigid edge spacer frames, revealing the control effect of edge structure on load distribution and plate deformation.

Although existing studies have made certain progress, there are still several deficiencies. Firstly, most existing experimental studies focus on small-size specimens or short-edge cold bending conditions, while full-scale experimental studies on the bending behavior of large-size monolithic tempered glass sheets subjected to long-edge deformation commonly used in engineering are relatively scarce. Compared with short-edge cold bending, long-edge cold bending is more prone to large deflection deformation, and its stress distribution and structural stability problems are more complex. Secondly, existing numerical studies are usually based on ideal initial geometric states, and rarely consider key factors, such as

tempered residual stress, initial self-weight deformation and contact nonlinearity at the same time, thus limiting the consistency between simulation results and actual engineering conditions. In addition, current design methods mainly rely on empirical indicators (such as warping ratio control) and lack bearing capacity calculation models with clear mechanical significance, which is difficult to meet the needs of complex engineering design.

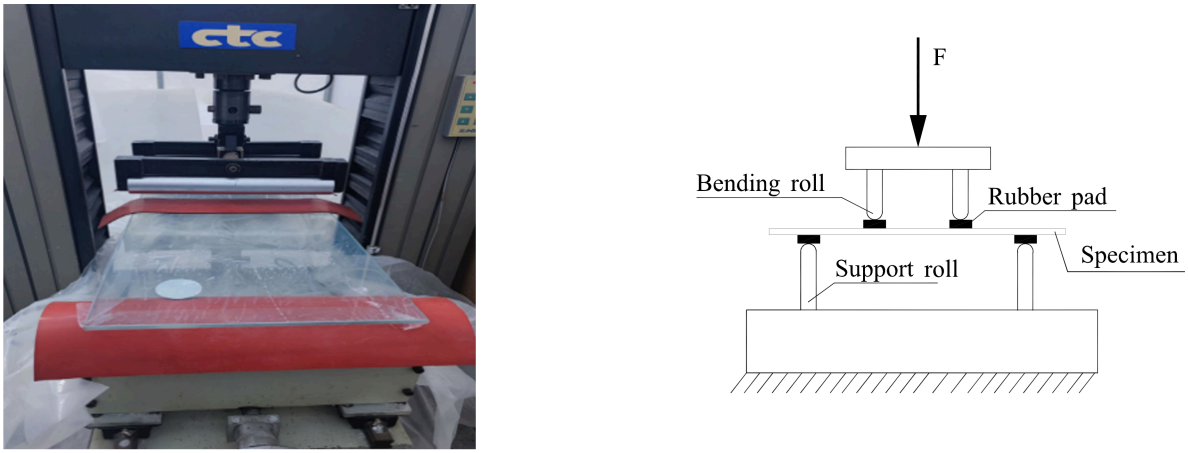
Based on the above research background, this paper takes monolithic tempered glass as the research object and carries out a systematic study around the long-edge cold bending condition. Firstly, the load-displacement response, stress development law and failure mode of glass during cold bending loading are obtained through full-scale tests. Secondly, a finite element model considering tempered residual stress, self-weight deformation and contact nonlinearity is established and verified by test results. On this basis, the influence laws of geometric parameters (length, width and thickness) on cold bending performance are further analyzed. The research results can provide a basis for the structural design and code improvement of flat tempered glass subjected to cold bending curtain walls.

2. Long-Edge Bending Tests of Flat Tempered Glass Sheets

2.1. Four-Point Bending Material Property Test of Tempered Glass

To obtain the basic flexural strength of tempered glass and provide a material failure criterion for the subsequent finite element analysis, four-point bending tests were carried out according to GB/T 37781-2019 [27]. Four-point bending loading can form a stable constant moment zone in the mid-span, which is convenient to obtain representative flexural strength indicators. The test specimens had dimensions of 1100 mm × 360 mm × 8 mm, and the edge processing technology was consistent with that of the cold bending test specimens to ensure the comparability of test results. The number of specimens was 10, and the number of valid specimens was 10. The measured flexural strength was 176.3 MPa with a standard deviation of 13.3 MPa, coefficient of variation (see Table 1). The obtained flexural strength was subsequently used as the equivalent tensile strength criterion to determine the failure state of tempered glass in the finite element model. The four-point bending test setup and loading configuration is shown in Figure 1.

The loading span and support span were selected according to GB/T 37781-2019 [27] to ensure a stable constant moment region in the middle section of the specimen.



(**a**) Test setup (**b**) Loading configuration

Figure 1. Four-point bending test setup and loading configuration.

Table 1. Four-point bending test results.

Specimen	Strength (Mpa)	Average Strength (Mpa)	Standard Deviation (Mpa)	Coefficient of Variation
1	160.3	176.3 Mpa	13.3 Mpa	7.54%
2	175.5			
3	185.7			
4	194.1			
5	187.7			
6	151.7			
7	166.4			
8	178.9			
9	185.6			
10	176.8			

2.2. Full-Scale Specimens

A total of three full-scale rectangular tempered glass specimens, designated as EG1~EG3, were used in this test. All specimens were made of architectural tempered glass with a plane size of 3200 mm × 1700 mm and a thickness of 8 mm. The specific parameters are shown in Table 2. The specimens were provided by Qibin Group (Heyuan, China), and their edges were mechanically polished to reduce the influence of edge defects on test results. The polishing process was consistent with actual engineering, and the glass used was from the same batch as that of the four-point bending test specimens in the previous section.

Table 2. Specimen dimensions.

Glass Type	Specimen ID	Plane Dimensions (mm)	Thickness (mm)	Average Surface Compressive Stress (MPa)
Tempered glass	EG1	3200 × 1700	8	−91.86
Tempered glass	EG2	3200 × 1700	8	−97.13
Tempered glass	EG3	3200 × 1700	8	−91.73

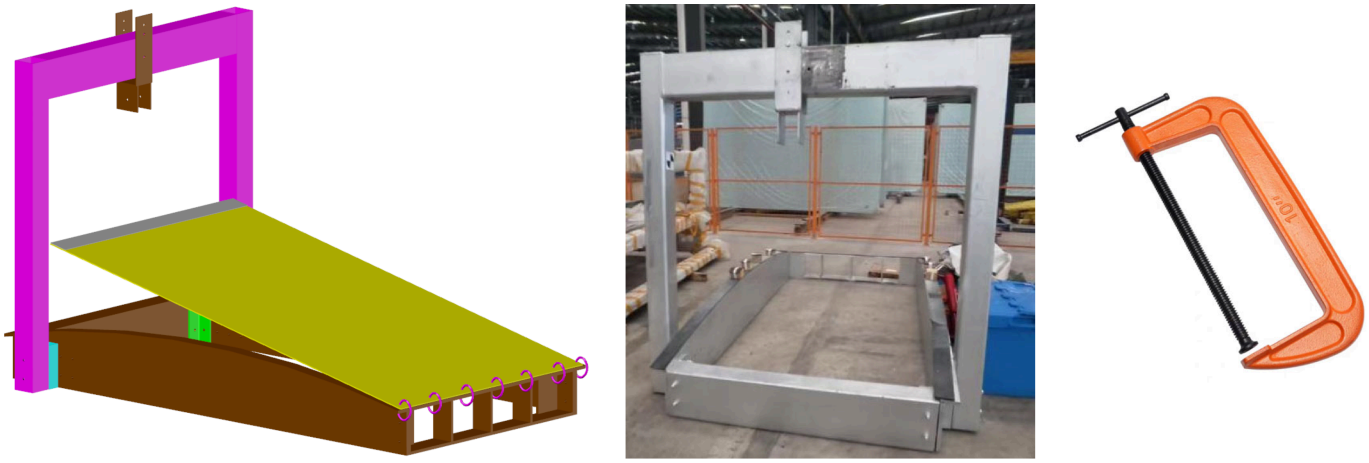
To verify the tempering quality, the fragment state was tested in accordance with GB 15763.2-2005 Safety glazing materials in building—Part 2: Tempered glass [28]. The results showed that the number of glass fragments in a 50 mm × 50 mm sampling area was 57, meeting the standard requirements.

2.3. Loading Setup and Boundary Conditions

According to the test requirements and glass specimen dimensions, a dedicated long-edge cold bending loading setup was designed and built, as shown in Figure 2. The setup mainly consists of three parts: a loading platform, loading equipment and boundary constraint components. The main body of the loading platform includes two curved guide rails with fixed curvature, two end support beams and a rigid gantry. The gantry is also used to fix the hand jack and the displacement meter mounting base.

The short edge at one end of the specimen was constrained by symmetrically arranged G-clamps to simulate actual support conditions. To avoid local damage caused by direct contact between the clamps and the glass surface, rubber pads were first laid on the upper surface of the glass, and then wooden blocks were placed on them, so that the G-clamps transmitted force indirectly through the wooden blocks. The G-clamp bolts were tightened gradually until the glass was just in contact with the rubber pads on the loading platform.

The clamping degree was controlled by the principle that there were no initial damages, such as indentations or edge chipping on the glass edge. No loosening, misalignment or identifiable slippage of the clamps was observed during the test, indicating that the boundary constraints were stable and reliable.



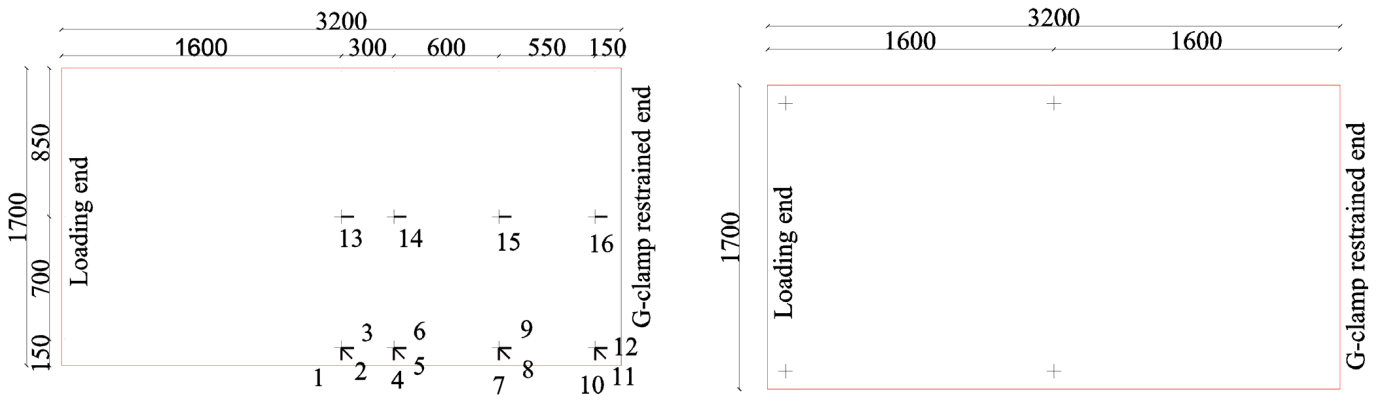
(**a**) Loading platform model (**b**) Loading platform physical setup (**c**) G-clamp

Figure 2. Long-edge cold bending test setup for glass.

This test is a short-term verification test for the long-edge bearing performance of cold-bent glass, with glass breakage as the test termination mark. The failure mechanism of glass is usually controlled by tensile stress, and the propagation of surface microcracks under tensile stress is the main cause of its failure. Its bearing capacity essentially depends on the ultimate tensile strength of the material. The current Technical Specification for Glass Curtain Wall Engineering in China adopts the first strength theory in glass strength design [29], taking whether the principal tensile stress at any point inside the glass exceeds the material strength limit as the failure criterion.

Based on this theory, to accurately study the mechanical response of cold-bent glass during loading, the strain measuring points in this test were mainly arranged in the areas where the tensile stress on the glass surface was expected to be large. According to the symmetry characteristics of the test loading method and combined with the analysis of failure modes of long-edge cold bending tests in existing studies [30], the failure area of glass usually appears in the front middle section of the specimen. Therefore, the arrangement of strain gauges is as shown in Figure 3: strain rosettes were set near the side edges of the glass specimen to obtain multi-directional strain states, and uniaxial strain gauges were arranged in the middle expected high tensile stress area.

Considering the boundary conditions and deformation characteristics of the long-edge bending configuration, the vertical displacement at the loading edge was selected as the primary deformation control parameter. During the test, one short edge of the glass specimen was constrained by G-clamps, and the position of this constrained region remained unchanged throughout the loading process. Therefore, the applied vertical displacement mainly induced bending deformation along the long-edge direction, which governed the overall mechanical response of the glass sheet. Other deformation components, such as lateral shifting, were limited by the boundary conditions and were not considered as the dominant deformation mode in this study.

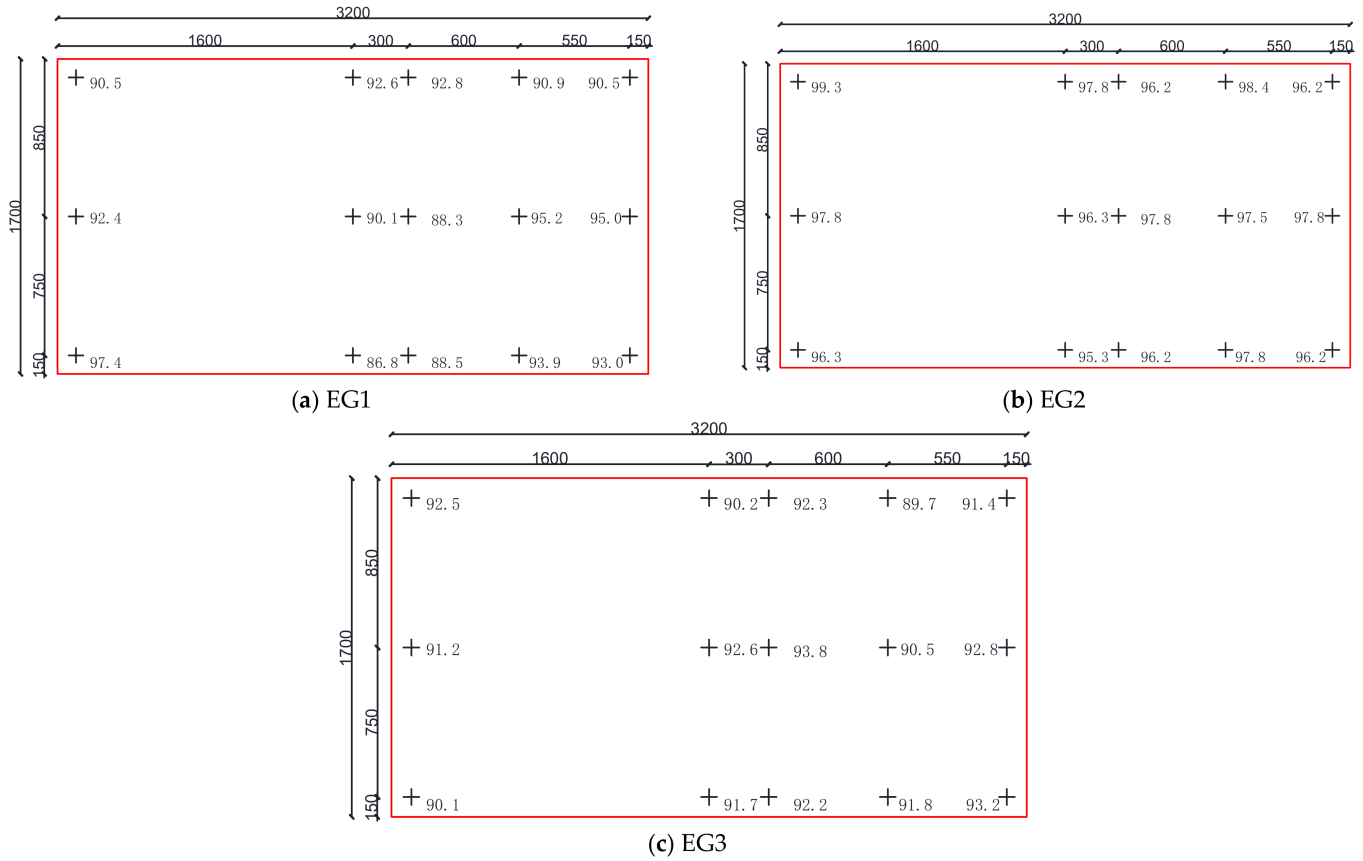


(**a**) Strain gauge measuring points (**b**) Displacement meter measuring points

Figure 3. Measuring point arrangement.

In addition to the vertical displacement at the loading end, the displacement changes at both long-edge midpoints and the constrained end were simultaneously recorded. These measurements were used to characterize the global deformation behavior, including the bending deformation and warping evolution of the glass sheet during long-edge bending.

This test takes glass breakage as the termination mark. The measurement system includes four parts: strain measurement, displacement measurement, geometric morphology measurement and initial tempered stress measurement. The initial tempered stress is shown in Figure 4.



(**a**) EG1 (**b**) EG2

(**c**) EG3

Figure 4. Initial tempered stress distribution.

2.4. Test Loading Procedure

For the 8 mm thick EG1~EG3 monolithic tempered glass specimens, a stepwise loading method by placing metal blocks was adopted to apply vertical gravity load. The specific loading procedure is as follows:

Debug the loading system and data acquisition system and complete zeroing; lay rubber pads on the surface of the loading platform steel frame as a buffer layer to avoid rigid contact between the glass and the steel frame; place the glass specimen on the loading platform by a combination of mechanical hoisting and manual positioning (see Figure 5), and install G-clamps according to the design requirements to complete boundary constraints; place metal blocks one by one on the loading end of the specimen, with a time interval of 1 min between consecutive metal blocks; when the load reaches the predetermined critical value, adjust the time interval to 5 min to allow the deformation to fully stabilize; continue loading until the specimen breaks, and record the failure load, failure displacement and failure mode.



Figure 5. Glass specimen installation site.

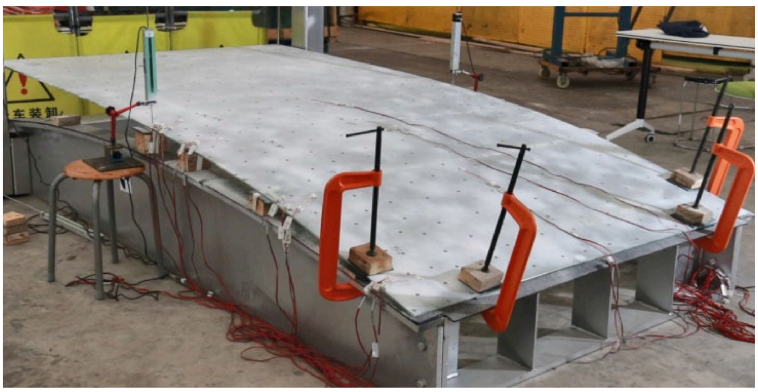
3. Test Results and Analysis

3.1. Failure Process and Failure Modes

The overall deformation of monolithic tempered glass was relatively smooth in the initial stage of cold bending loading, and no obvious slippage was observed at the clamps and pads. As the load increased, the bending deformation of the specimen was concentrated in the mid-span area of the loading end, and the strain at the dangerous point increased gradually with displacement. When approaching the ultimate state, the strain record showed a sudden increase accompanied by the rapid propagation of visible cracks, showing typical brittle failure, as shown in Figure 6. Once fracture occurred, the tempered glass specimens experienced instantaneous fragmentation due to the release of stored elastic energy associated with the residual stress field. The failure process exhibited typical brittle fracture characteristics, with no apparent load degradation before failure.



(**a**) Specimen before loading



(**b**) Specimen clamped by G-clamp



(**c**) Specimen at 605 N load



(**d**) Specimen at failure moment

Figure 6. Failure process of flat tempered glass sheets during long-edge bending.

3.2. Ultimate Bearing Capacity and Deformation Characteristics

The key parameters of the three specimens at the failure of the dangerous point are shown in Table 3. The failure loads of monolithic tempered glass specimens under long-edge cold bending ranged from 580 N to 705 N, with an average value of 630 N; the failure displacements ranged from 219 mm to 244 mm, with an average value of 231 mm. It should be noted that the measured failure load represents the ultimate bearing capacity of the cold-bent glass system under the specific loading and boundary conditions adopted in this study, rather than the intrinsic material strength of tempered glass. The principal stresses calculated from the strain measurements at the monitoring points near the expected critical region ranged from 63.32 MPa to 70.24 MPa. It should be noted that these values represent the stress state at the strain-gauge locations rather than the absolute maximum stress of the glass. Moreover, the stress calculated from the measured strain does not include the tensile stress contribution caused by the self-weight-induced deformation of the glass sheet. The coefficients of variation (COV) of failure strain, failure stress, failure displacement and failure load were 5.74%, 5.74%, 5.40% and 10.50%, respectively. The relatively low COV values indicate acceptable consistency and relatively low dispersion among the three full-scale specimens under identical loading and boundary conditions. Considering the limited number of full-scale specimens, the statistical analysis in this study was mainly performed to evaluate the repeatability of test results, rather than to establish a statistical strength distribution. Among them, specimen EG3 had the largest failure load, failure displacement and failure warping value, indicating that its ultimate bearing capacity and deformation capacity were relatively stronger. It is worth noting that the failure warping ratios of all specimens ranged from 0.105 to 0.114, which are significantly higher than the current design control value of 0.025, indicating that the existing design indicators are relatively conservative and cold-bent glass has a large safety reserve.

Table 3. Failure characteristic parameters of dangerous points of tempered glass specimens.

Specimen	Failure Strain ε_u (με)	Failure Stress (MPa)	Failure Displacement δ_u (mm)	Failure Load P_u (N)
EG1	879.43	63.32	219	580
EG2	975.59	70.24	231	605
EG3	890.82	64.14	244	705
Mean	915.28	65.90	231	630
Standard deviation	52.54	3.78	12	66
COV	5.74%	5.74%	5.40%	10.50%

The quantities are defined and their symbols are given as follows, which are directly represented by symbols in the table. The failure strain is denoted as με, which takes the strain value immediately before the sudden change in the strain acquisition record; the vertical displacement at the loading end at failure is denoted as δ_u, which takes the average value of the readings of the two displacement meters at the loading end; the failure load is denoted as P_u, which takes the vertical force value immediately before the sudden change in the load sensor record.

3.3. Experimental Load-Displacement Curve Analysis

The load-displacement curves of the three monolithic tempered glass specimens under long-edge cold bending showed an overall continuous upward trend, as shown in Figure 7. No obvious load degradation occurred before failure, and all specimens terminated with sudden fracture. The three curves almost coincided in the small displacement stage, indicating good consistency in the initial stiffness of specimens of the same specification under the same boundary and loading conditions. Taking vertical displacements of 60 mm, 120 mm and 180 mm as boundaries, the response process can be divided into an initial stage, a transition stage and a strengthening stage. The curve was approximately linear in the range of 0~60 mm, and the load increased steadily with displacement; the slope of the curve gradually increased after 60~120 mm; the slope further increased in the range of 120~180 mm, indicating that the structural stiffness was enhanced in the large displacement stage. After 180 mm, the dispersion of each curve increased and terminated at different displacements, reflecting that the ultimate state was more significantly affected by the randomness of edge microdefects and cracks.

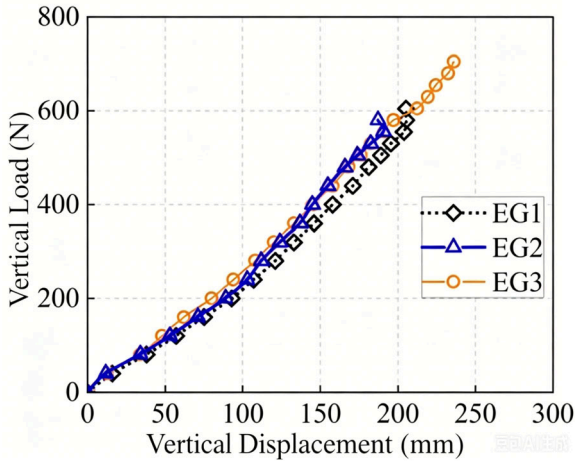


Figure 7. Load-displacement curves of flat tempered glass sheets during long-edge bending.

4. Finite Element Simulation and Parametric Analysis

4.1. Finite Element Simulation Process

A finite element model consistent with the test specimen specifications was established in this numerical simulation, and its geometric dimensions were completely the same as those of the test specimens. The specific dimension parameters are shown in Table 2. To reflect the stress state during the test as realistically as possible, all components in the model were modeled using deformable three-dimensional solid elements, including tempered glass plates, wooden blocks and steel frames. Through solid modeling of each component, the contact relationships, deformation characteristics and stress distribution of the specimen during loading can be simulated more accurately. At the same time, the materials involved in the model were defined according to the actual performance parameters of the test materials, and the main material property parameters are shown in Table 4.

Table 4. Material properties.

Material	Elastic Modulus (N/mm^2)	Poisson's Ratio	Density (t/m^3)
Tempered glass	72,000	0.22	2.56
Wood	10,000	0.30	0.5
Steel frame	206,000	0.30	7.85

The component assembly of the finite element model was completed according to the actual arrangement of the glass specimen, wooden blocks and loading platform during the test. The assembly method, component position relationship and overall arrangement of each model were consistent with the experimental setup. To improve the readability of the numerical model, different colors were assigned to distinguish the main components in Figure 8.

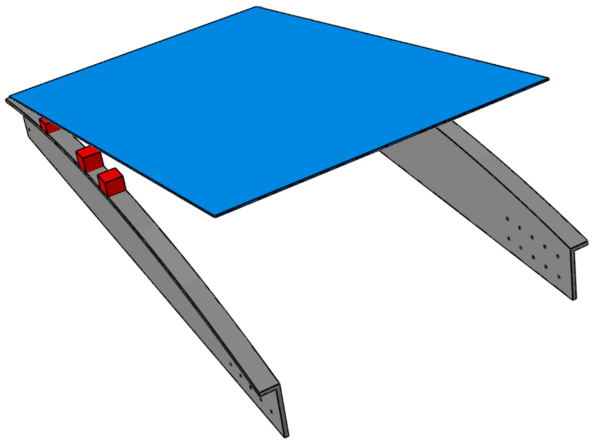


Figure 8. Finite element model assembly with different component representations.

The finite element model was established according to the actual stress state and contact relationship of the specimen during the test. In the test, the glass and wooden blocks were in contact through rubber pads. The primary function of the rubber pads was to reduce local contact stress concentration and prevent premature glass failure caused by direct rigid contact. During the test, the vertical deformation of the rubber pads under the applied pressure of the glass specimen was very small, indicating that their influence on the overall deformation response was limited. Therefore, the rubber pads were simplified in the FE model, while the contact interaction between the glass and wooden blocks was retained to consider the boundary effects. A surface-to-surface contact form was adopted between

them, and according to the principle that the surface with larger stiffness is defined as the master surface, the glass surface was set as the master surface and the wooden block surface as the slave surface. In the contact properties, the normal behavior adopted hard contact, and the tangential behavior adopted the penalty friction model with a friction coefficient of 0.4. This value was selected based on the typical friction characteristics of glass–wood contact in engineering applications. During the test, no obvious sliding between the glass specimen and wooden blocks was observed, indicating that the selected friction coefficient can reasonably describe the contact condition.

To facilitate the application of boundary conditions and loads, reference points R3 and R4 were created at the midpoints of the two short edges of the glass, respectively. Among them, reference point R3 established a coupling constraint with the surface area of the constrained end short edge of the glass, and reference point R4 established a coupling constraint with the surface area of the loading end short edge of the glass, to establish the motion coordination relationship between the reference points and the corresponding areas, thereby realizing the unified application of constraint conditions and loading effects.

The boundary conditions and load application method of the finite element model were determined according to the actual constraint state and loading process of the test setup. Among them, reference point R3 was used to simulate the boundary conditions of the constrained end of the specimen. After establishing the coupling constraint between the surface area of the constrained end short edge of the glass and reference point R3, the translational degrees of freedom in the X, Y and Z directions and the rotational degrees of freedom about the Y and Z axes were constrained at reference point R3 to simulate the clamping constraint effect of G-clamps on the glass short edge in the test. This boundary condition can reflect the actual stress characteristics of limited displacement and constrained rotation at the constrained end as a whole, and at the same time avoid non-real stress concentration that may be caused by directly applying constraints to local nodes, making the boundary simulation closer to the test conditions.

Reference point R4 was used to apply external loads. After establishing the coupling constraint between the surface area of the loading end short edge of the glass and reference point R4, a vertical displacement load was applied at reference point R4 to simulate the loading process of gradually applying displacement to the specimen short edge by the jack in the test. Adopting displacement control loading is consistent with the test process on the one hand, and on the other hand, it is conducive to improving the stability of numerical calculation and can obtain the complete load-displacement response relationship of the specimen during the entire loading process.

Considering that the glass specimen has obvious large deflection deformation during cold bending loading, and the contact state between the glass and the wooden blocks will be continuously adjusted with the loading process, nonlinear effects were considered in the model analysis. Specifically, the geometric nonlinear option was turned on in the analysis to reflect the changes in structural stiffness and internal force distribution during the deformation development; at the same time, combined with the surface contact relationship defined between the glass and the wooden blocks, the influence of contact nonlinearity on the stress response was considered. Thus, the stress and deformation characteristics of the specimen during actual cold bending loading can be simulated more realistically.

Tempered glass forms a self-equilibrium residual stress field along the thickness direction during the quenching process, and its typical distribution characteristic is that the surface layer is under compression and the core is under tension. To consider this influence in finite element analysis, this paper equated the tempered residual stress to the initial stress field in the solid model. Considering that the application of continuously distributed residual stress is relatively complex in numerical implementation, a simplified method

of three-layer segmentation along the thickness direction was adopted for simulation. For 8 mm thick tempered glass, it was divided into an upper surface compressive stress layer, a middle tensile stress layer and a lower surface compressive stress layer along the thickness direction, where the thickness of the single-side surface layer was 1.6 mm and the thickness of the middle layer was 4.8 mm. The thickness layering schematic and initial stress application are shown in Figure 9.

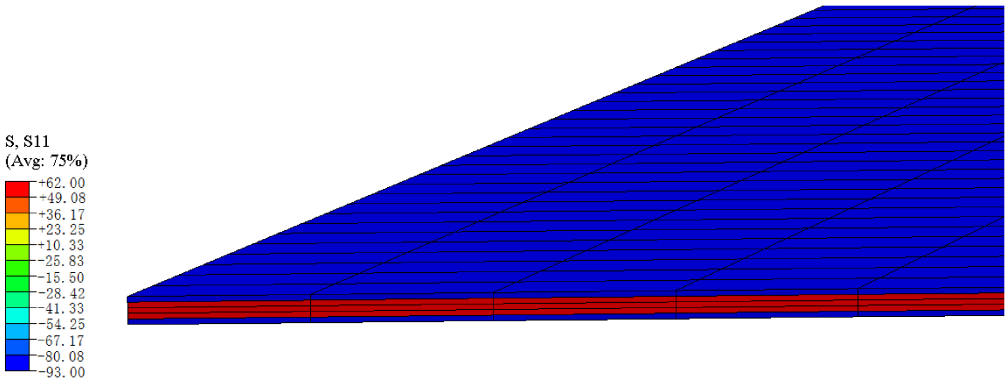


Figure 9. Initial stress application of tempered glass.

The measured surface compressive stresses of EG1–EG3 were 91.86 MPa, 97.13 MPa and 91.73 MPa, respectively. Considering the relatively small variation among the specimens and the objective of evaluating the global mechanical response, an average value of 93 MPa was adopted as the representative surface compressive stress in the FE model. To ensure that the initial residual stress field satisfies the self-equilibrium condition along the thickness direction, the middle tensile stress was determined to be 62 MPa according to the zero resultant force on the section. Therefore, when assigning initial stresses, in-plane residual compressive stresses of −93 MPa were applied to the upper and lower surface layers respectively, and an in-plane residual tensile stress of 62 MPa was applied to the middle layer, with all other stress components set to 0. Through the above treatment, the typical residual stress distribution characteristic of "surface compression and core tension" of tempered glass can be reasonably reflected while ensuring the simplicity of the model. Although the actual residual stress profile is nonlinear, the simplified three-layer model can reasonably represent the stress characteristics of tempered glass and is suitable for evaluating the global mechanical response of cold-bent glass.

To balance calculation accuracy and efficiency, targeted mesh generation was carried out for the model combined with the geometric characteristics, material properties and stress characteristics of each component. Overall, all components of the model were discretized using three-dimensional solid elements, among which glass, as the main stress-bearing component, adopted higher-order elements and was appropriately refined; PVB interlayers, due to their small thickness, adopted finer mesh generation; and spacer bars adopted relatively coarser meshes according to their structural function and dimensional characteristics. Taking monolithic glass as an example, the mesh generation result of the finite element model is shown in Figure 10.

The glass plate adopted 20-node quadratic reduced-integration three-dimensional solid elements C3D20R with a mesh size of 50 mm. This element can well describe the bending deformation and stress distribution characteristics of glass during cold bending loading, and is suitable for solid components, such as glass plates that are mainly subjected to bending stress. Combined with the relatively regular geometric shape of glass, its mesh generation was dominated by regular hexahedral meshes, and the mesh distribution on the plate surface was relatively uniform, which is conducive to improving calculation

accuracy and can reduce the adverse effect of mesh distortion on calculation results to a certain extent.

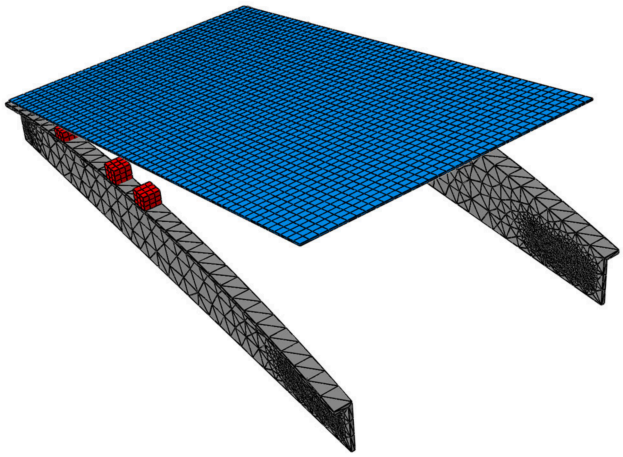


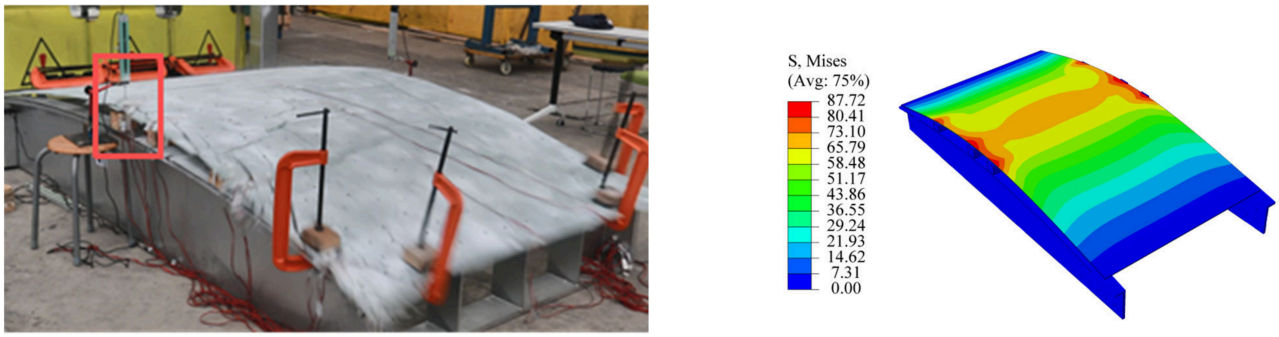
Figure 10. Mesh generation of tempered glass.

The steel frame and wooden blocks were mainly used to simulate the support and loading conditions in the test and were not the key research objects of this paper. Therefore, their mesh generation was based on the principles of meeting geometric adaptability, contact calculation stability and overall convergence requirements, and the specific mesh forms will not be described in detail.

4.2. Comparison of Simulation Results

In ABAQUS, the failure judgment of brittle materials can usually adopt the maximum stress criterion or the maximum strain criterion. Among them, the maximum stress criterion takes whether a certain stress component inside the material reaches its strength limit as the failure basis; when any stress component exceeds the corresponding strength, the material is considered to have failed. The maximum strain criterion takes whether the strain reaches the ultimate strain of the material as the judgment standard; when a certain strain component exceeds the allowable range, the material is also considered to have failed. Combined with the stress characteristics of tempered glass and existing test research results, this paper adopted a judgment method based on the maximum surface stress of glass to analyze the failure state of tempered glass and determine its failure load accordingly. Tempered glass is a typical brittle material with an elastic modulus of 72000 MPa and a Poisson's ratio of 0.22. During the stress process, its stress–strain relationship is basically linearly elastic before failure, and there is no obvious yield and plastic development stage similar to metal materials. Therefore, it is difficult for the internal structure to achieve stress redistribution through plastic deformation. When the tensile stress on the glass surface reaches the ultimate value, cracking often occurs rapidly and leads to overall failure. In this study, the four-point bending strength was adopted as an equivalent strength criterion for numerical evaluation. Although the four-point bending test does not directly measure the edge strength of the full-scale specimen, the specimens were manufactured using the same batch of glass material, thickness and edge processing method. Therefore, the measured strength incorporates, to some extent, the influence of material and processing quality and provides a reasonable equivalent strength parameter for evaluating the failure behavior in FE analysis. The difference between material strength obtained from four-point bending and failure stress under cold bending conditions is discussed in Section 2. The finite element model considers the self-weight deformation of the glass specimen; therefore, the simulated maximum tensile stress represents the combined effect of external loading and

self-weight, which cannot be directly compared with the strain-gauge-based experimental stress. Comparison of failure contours and test diagrams of glass models are listed in Figure 11.



(**a**) Test failure diagram of glass (**b**) Simulated failure contour of glass

Figure 11. Comparison of failure contours and test diagrams of glass models.

It can be seen from the experimental strain response and finite element stress contours in Figure 11 that the maximum stress regions are mainly concentrated near the mid-edge area close to the wooden block. The location of the high-stress region predicted by the FE model is consistent with the area showing significant strain response during the test, indicating that this region governs the failure behavior under the present boundary conditions. It should be noted that the maximum stress predicted by the FE model does not necessarily coincide exactly with the strain gauge location. Therefore, the stress calculated from experimental strain measurements represents the local stress state at the monitoring position rather than the absolute peak stress of the glass.

The main reason for the above phenomenon is that the glass plate undergoes large deflection bending deformation as a whole during cold bending loading, the mid-span area is subjected to the most significant bending effect, and the edge part is more sensitive to changes in tensile stress. At the same time, local stress is more likely to concentrate near the wooden block due to the influence of contact and constraint conditions, making this area a dangerous part where cracks preferentially initiate. Although there are certain differences in the fragmentation morphology and remaining integrity after failure among the four types of glass, their initial failure positions are basically consistent, indicating that the dangerous areas of various glass specimens have good uniformity under the test conditions of this paper. The finite element model can accurately predict the failure initiation position, indicating that the established model has good rationality in terms of contact relationship, boundary conditions and failure judgment.

4.3. Comparison of Failure Load and Failure Vertical Displacement

Table 5 shows the comparison results between the test values and simulated values of failure loads and vertical displacements of the four types of glass specimens. Overall, the prediction results of the finite element model for failure loads are in good agreement with the test results. The average absolute error of failure loads for 12 specimens is 4.94%, and the errors of most specimens are controlled within 10%, indicating that the model can well reflect the ultimate bearing capacity of different structural types of glass specimens under cold bending. From the results of each group, the dispersion of the monolithic tempered glass group is relatively large, while the simulation results of the laminated glass, insulating glass and insulating laminated glass groups are closer to the test results.

Table 5. Comparison of failure loads and peak displacements.

Specimen	Comparison of Failure Loads			Comparison of Peak Displacements		
	Test Value (N)	Simulation Value (N)	Error (%)	Test Value (mm)	Simulation Value (mm)	Error (%)
EG1	580	640	10.34	219	231	5.48
EG2	605	640	5.79	231	231	0.00
EG3	705	640	−9.22	244	231	−5.33

The comparison results of vertical displacements show that the finite element model also has good predictive ability for the overall deformation level of the specimens. The average absolute error of vertical displacements for 12 specimens is 5.01%, and except for individual specimens with relatively large deviations, the other results are relatively close to the test values. Compared with failure loads, vertical displacement indicators are more sensitive to test installation accuracy, wooden block contact state, clamping tightness and the dispersion of actual mechanical parameters of the interlayer, so it is reasonable that their errors are slightly larger than those of load indicators. The finite element model can not only well predict the failure load of the specimen, but also reflect its deformation response characteristics as a whole, indicating that the model has good applicability in both bearing capacity and deformation.

4.4. Load-Displacement Curve Analysis

Figure 12 shows the comparison between the test results and finite element results of the load-displacement curves of glass specimens under long-edge cold bending. Overall, the finite element curves are consistent with the test curves in terms of change trend, and the agreement is good in the initial loading stage, indicating that the model can accurately reflect the initial stiffness and overall stress characteristics of the specimen; as the displacement increases, some specimens show certain deviations in the middle and late stages, but the simulation curves are still relatively close to the test results as a whole.

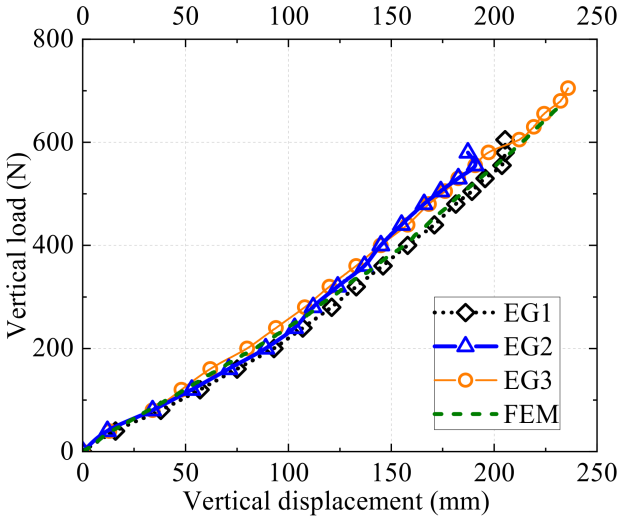


Figure 12. Comparison of load-displacement curves of glass.

The finite element results are in good agreement with the test results; the dispersion of monolithic glass is relatively large, and the deviation of individual specimens is more obvious in the ultimate stage.

The deviations between the test and simulation mainly come from the following aspects: first, edge microdefects, initial damage and processing dispersion of glass will

affect the ultimate bearing capacity, while the model adopts ideal geometry and uniform material parameters without considering their random distribution; second, the actual contact state between wooden blocks, rubber pads and clamps in the test is more complex, and local compression and clamping differences will affect the load transfer in the middle and late stages. Overall, the finite element model can well reflect the overall mechanical response of different structural glasses under long-edge cold bending conditions, but there are still certain limitations in the characterization of local random failure behavior near the ultimate state.

Through the comparative analysis of failure position, failure load and vertical displacement, and load-displacement curves, it can be seen that the long-edge cold bending finite element results are in good agreement with the test results as a whole. The initial failure positions of the glass specimens are all located near the wooden block at the mid-edge, and the simulated high-stress area is basically consistent with the test crack initiation position; the average absolute errors of failure load and vertical displacement are 4.94% and 5.01% respectively, indicating that the established model can well reflect the overall bearing capacity and deformation level of different structural glass specimens.

The comparison of load-displacement curves shows that the finite element model can well reflect the stiffness characteristics of the specimen in the initial loading stage and the overall bearing development trend in the middle and late stages. The deviations between the test and simulation are mainly concentrated in the ultimate stage, which is mainly related to the randomness of glass edge microdefects and initial damage, the difference in contact states of wooden blocks and clamps, and the simplified modeling of interlayers and insulating layers. Overall, the model established in this paper can be used to analyze the overall mechanical response laws of different structural glasses under long-edge cold bending conditions, but the characterization of local random failure behavior near the ultimate state still needs to be comprehensively judged in combination with test results.

4.5. Parametric Analysis

To further analyze the influence of geometric dimension parameters on the long-edge cold bending mechanical response of monolithic tempered glass and provide a finite element basis for the subsequent long-edge cold bending theoretical model, dimensional parameter analysis was carried out based on the validated finite element model. The analysis object was selected as the monolithic tempered glass long-edge cold bending model, and the material properties, boundary conditions, contact relationships and loading methods were consistent with the aforementioned finite element model, only changing two geometric parameters of glass width and thickness.

Taking the monolithic tempered glass specimen size of 3200 mm × 1700 mm × 8 mm in the test as the baseline model, a single-factor analysis method was adopted, that is, only one dimension parameter was changed each time while keeping the other parameters at the baseline values. The glass widths were taken as 1300 mm, 1700 mm and 2100 mm, respectively; the glass thicknesses were taken as 6 mm, 8 mm and 10 mm, respectively. The parameter conditions are shown in Table 6.

This section mainly extracts the vertical load-displacement curves at the loading end of each working condition, and analyzes the influences of width and thickness on the overall long-edge cold bending response of monolithic tempered glass from the aspects of curve slope, load growth trend and bearing level. It should be noted that only monolithic tempered glass was selected as the object in this parametric analysis, mainly because monolithic glass is the basic component unit of laminated glass, insulating glass and insulating laminated glass, and its stress path is relatively clear, which can avoid the

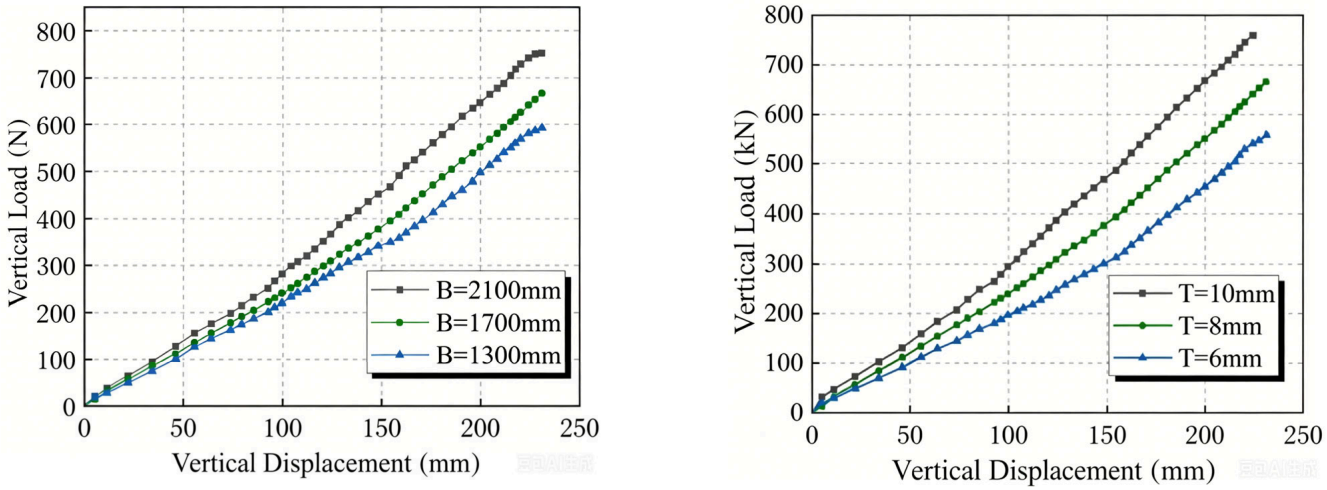
interference of factors, such as interlayer synergy, edge structure of insulating layer and interlayer interaction on the dimensional parameter laws.

Table 6. Dimensional parameter analysis conditions of tempered glass.

Working Condition	Length (mm)	Width (mm)	Thickness (mm)
Baseline model	3200	1700	8
B-1	3200	1300	8
B-2	3200	2100	8
T-1	3200	1700	6
T-2	3200	1700	10

To investigate the effects of geometric parameters on the long-edge cold bending behavior of monolithic tempered glass, a parametric study was conducted based on the validated FE model. Only glass width and thickness were varied, with other conditions identical to the baseline model (3200 mm × 1700 mm × 8 mm). The width ranged from 1300 mm to 2100 mm, and the thickness ranged from 6 mm to 10 mm, as detailed in Table 5.

As shown in Figure 13a, all load-displacement curves exhibit a continuous upward trend with no load degradation, indicating that width variation does not alter the fundamental response law. Increasing width from 1300 mm to 2100 mm shifts the curve upward slightly, with the load at the same displacement increasing moderately. However, the load does not increase proportionally with width, as only a portion of the plate width effectively participates in load bearing. Thus, width has a limited positive effect on bearing capacity.



(**a**) Width parameter (**b**) Thickness parameter

Figure 13. Numerical load-displacement curves under different geometric parameters.

Figure 13b shows that thickness has a much more pronounced influence. Increasing thickness from 6 mm to 10 mm significantly shifts the curve upward, leading to a substantial increase in bearing capacity. At a displacement of 220 mm, the load for the 10 mm thick specimen exceeds 700 N, compared to approximately 500 N for the 6 mm thick specimen. The gap between curves widens with increasing displacement, indicating that thickness has a more significant effect in the large deformation stage.

Mechanically, the bending stiffness of glass is proportional to the cube of thickness, making thickness the dominant parameter controlling long-edge cold bending performance. While increasing thickness effectively improves bearing reserve, it also increases self-weight and installation difficulty, requiring comprehensive consideration in engineering design.

5. Conclusions

This paper presents a systematic investigation on the mechanical behavior, failure characteristics and parametric sensitivity of large-size monolithic tempered glass (3200 mm × 1700 mm × 8 mm) under long-edge cold bending, through full-scale tests, refined FE simulation and geometric parameter analysis. The main conclusions are as follows:

1. Monolithic tempered glass under long-edge cold bending exhibits typical brittle failure. Failure was associated with the high-stress region at the mid-edge near the wooden block, where the FE-predicted stress concentration and measured strain response indicated critical behavior. The failure loads range from 580 N to 705 N, and failure displacements range from 219 mm to 244 mm, with good test repeatability.
2. The load-displacement curves show a continuous ascending trend with stiffness enhancement in the large-deflection stage due to the membrane effect. The failure warping ratios are significantly higher than current code limits, indicating that existing deformation control indices are conservative and cold-bent glass has sufficient safety reserve.
3. The proposed FE model, incorporating initial tempered residual stress, self-weight deformation and contact nonlinearity, accurately predicts failure location, ultimate load and displacement, with average simulation errors below 4.94% and 5.01%, respectively.
4. Parametric analysis reveals that glass thickness is the most critical factor affecting long-edge cold bending capacity, while width has a relatively limited positive effect.
5. Local stress concentration near the boundary region may influence the failure behavior of long-edge cold-bent glass. Special attention should be paid to edge finishing, constraint block arrangement and uniform clamping in engineering practice.

The findings provide experimental support and numerical basis for the design and safety evaluation of large-size long-edge cold-bent glass curtain walls, and offer a reference for improving relevant design codes.

Author Contributions: Conceptualization, W.L., J.M., J.Z. and X.Z.; Methodology, W.L., W.C., J.Z. and X.Z.; Software, W.L., J.M. and W.C.; Validation, W.L., W.C. and X.Z.; Formal analysis, W.L., W.C. and X.Z.; Investigation, W.L., W.C. and W.W.; Resources, J.M. and H.C.; Data curation, H.C.; Writing—original draft preparation, W.L. and W.C.; Writing—review and editing, W.L., W.C., H.C. and W.W.; Visualization, W.L., J.Z., H.C. and W.W.; Supervision, J.M., J.Z., X.Z., H.C. and W.W.; Project administration, J.M., J.Z., X.Z. and W.W.; Funding acquisition, W.L., J.Z. and X.Z. All authors have read and agreed to the published version of the manuscript.

Funding: The work is supported partly by the China Postdoctoral Science Foundation (No. 2025M774323).

Data Availability Statement: The original contributions presented in this study are included in the article. Further inquiries can be directed to the corresponding author.

Conflicts of Interest: Author Jie Ming was employed by the company Shenzhen Bay Area Urban Construction and Development Co., Ltd. Author Jianghao Zhou, Hualin Cao, Wei Wei were employed by the company China Construction Buer Curtain Wall & Decoration Co., Ltd. The remaining authors declare that the research was conducted in the absence of any commercial or financial relationships that could be construed as potential conflicts of interest.

References

1. Yang, R. Application of cold bending technology in curved glass curtain wall. *Doors Windows* **2015**, *9*, 14–15. (In Chinese)
2. Fan, Y.B. Research on application of cold bent glass technology in a natatorium project. *Eng. Qual.* **2017**, *35*, 72–74. (In Chinese)
3. Sun, J.; Jin, Z.Q. Construction technology and fatigue performance test of frame-supported cold bent glass for the daylighting roof of Suzhou Center. *Constr. Technol.* **2019**, *48*, 129–133. (In Chinese)

4. Huang, J. Design and construction analysis of cold bent curtain wall unit panels. *Archit. Tech.* **2021**, 197–200. (In Chinese) [CrossRef]
5. Li, S.L.; Shi, G.; Wang, F.Z.; Zhao, H.T.; Li, X.Q.; Wang, D.X.; Zhang, C.H.; Jia, Y.Q. Research on cold bending performance of glass curtain wall of Oujia Building. *Build. Struct.* **2026**, 1–6. (In Chinese) [CrossRef]
6. Eekhout, M.; Niderehe, S. The cold bent glass roof of the Victoria & Albert Museum, London. In *Proceedings of the Challenging Glass 2 Conference on Architectural and Structural Applications of Glass*; Bos, F., Louter, C., Veer, F., Eds.; Delft University of Technology: Delft, The Netherlands, 2010; Volume 2, pp. 139–148.
7. Gavriil, K.; Guseinov, R.; Pérez, J.; Pellis, D.; Henderson, P.; Rist, F.; Pottmann, H.; Bickel, B. Computational design of cold bent glass façades. *ACM Trans. Graph.* **2020**, *39*, 208. [CrossRef]
8. Laurs, M.; Feldmann, M. Contribution to the design of cold bent glass. *Glass Struct. Eng.* **2025**, *10*, 2. [CrossRef]
9. Mazzucchelli, E.S.; Ancillotti, A.; Lucchini, A. The engineering of free forms envelopes: The case of the Hadid Tower twisting shape façade. In Proceedings of the 41st IAHS World Congress on Housing: Sustainability and Innovation for the Future, Albufeira, Portugal, 13–16 September 2016; pp. 1–10.
10. Jiang, J.L. Mechanical Behavior and Design Method of Unidirectional Cold Bent Insulating Tempered Glass Panels. Ph.D. Thesis, Guangxi University, Nanning, China, 2018. (In Chinese)
11. Li, J.W. Research on Forward Mechanical Performance of Unidirectional Cold Bent Insulating Laminated Glass Panels. Master's Thesis, Guangxi University, Nanning, China, 2020. (In Chinese)
12. Zhang, X.D.; Luo, D.; Li, J.W.; Long, Y.J. Experimental study on mechanical response of unidirectional cold bent insulating laminated glass panels. *Ind. Constr.* **2022**, *54*, 159–165. (In Chinese)
13. Xu, Z.L.; Zhang, E.M.; Zhang, X.D.; Jiang, J.L. Experimental study on stress distribution measurement of cold bent insulating glass panels using optical fiber method. *China Meas. Test.* **2022**, *48*, 29–34. (In Chinese)
14. Jin, X. Research on Forward Mechanical Performance and Design Method of Cold Bent Twisted Laminated Glass Panels. Master's Thesis, Guangxi University, Nanning, China, 2016. (In Chinese)
15. Zhang, X.; Zhou, W.; Xu, M. Experimental study on single corner cold bending mechanical response of laminated PVB interlayer tempered glass panes and the coupling effect with load. *Materials* **2021**, *14*, 6914. [CrossRef] [PubMed]
16. Beer, B. Options for complex geometry façades—Single corner vs. free form cold-bending. In Proceedings of the Glass Performance Days, Tampere, Finland, 26–28 June 2019; pp. 15–18.
17. Rahimzadeh, K.; Levelle, E.; Douglas, J. Extreme cold-bending: Geometric considerations and shape prediction with machine learning. In *Challenging Glass 8 Conference on Architectural and Structural Applications of Glass*; Belis, J., Bos, F., Louter, C., Eds.; Ghent University: Ghent, The Netherlands, 2022; Volume 8.
18. Wang, W.N.; Wang, Y.Z.; Han, X.Y.; Zou, Y. Research on strength safety evaluation of curved laminated insulated glass considering cold bending forming. In Proceedings of the Innovation and Development of Building Doors, Windows and Curtain Walls, Shanghai, China, 14–15 October 2024; pp. 204–218. (In Chinese)
19. Wang, W.N.; Han, X.Y.; Wang, Y.Z.; Zou, Y. Simplified calculation of glass stress considering cold bending effect. In Proceedings of the Innovation and Development of Building Doors, Windows and Curtain Walls, Shanghai, China, 1–2 August 2023; pp. 169–182. (In Chinese)
20. Sun, J.; Jin, Z.Q. Reliability research and construction technology of frame-supported cold bent glass. *Constr. Technol.* **2019**, *48*, 129–133. (In Chinese)
21. Datsiou, K.C.; Overend, M. The mechanical response of cold bent monolithic glass plates during the bending process. *Eng. Struct.* **2016**, *117*, 575–590. [CrossRef]
22. Laurs, M. Numerical and experimental investigations on the inherent stress state of cold-bent glass. In *Challenging Glass 7 Conference on Architectural and Structural Applications of Glass*; Belis, J., Bos, F., Louter, C., Eds.; Ghent University: Ghent, The Netherlands, 2020; Volume 7.
23. Galuppi, L.; Riva, E. Experimental and numerical characterization of twisting response of thin glass. *Glass Struct. Eng.* **2022**, *7*, 45–69. [CrossRef]
24. Zhang, X.; Liang, J.; Huang, D. Study on the mechanical response of anticlastic cold bending insulating glass and its coupling effect with uniform load. *PLoS ONE* **2021**, *16*, e0250463. [CrossRef] [PubMed]
25. Pölzl, F. Mechanical Behavior of Cold-Bent Insulating Glass Units. Master's Thesis, Graz University of Technology, Graz, Austria, 2017.
26. Van Driel, T.; Noteboom, C.; Overend, M. Investigations on the cold bending behaviour of a double glazing unit with a rigid edge-spacer frame. In *Proceedings of the Challenging Glass Conference*; TU Delft Open: Delft, The Netherlands, 2022; Volume 8.
27. *GB/T 37781-2019*; Test Method for Bending Strength of Glass Materials. China Standards Press: Beijing, China, 2019. (In Chinese)
28. *GB/T 15763.2-2025*; Safety Glass for Buildings—Part 2: Tempered Glass. China Standards Press: Beijing, China, 2025. (In Chinese)

29. *JGJ 102-2003*; Technical Code for Glass Curtain Wall Engineering. Ministry of Construction of the People's Republic of China: Beijing, China; China Architecture & Building Press: Beijing, China, 2003. (In Chinese)
30. Zhang, X.; Zou, C.; Yin, X. An experimental study on cold-bending stress and its reverse-coupling effect with the uniform load on cold-bent SGP laminated glass. *Appl. Sci.* **2021**, *11*, 10073. [CrossRef]

Disclaimer/Publisher's Note: The statements, opinions and data contained in all publications are solely those of the individual author(s) and contributor(s) and not of MDPI and/or the editor(s). MDPI and/or the editor(s) disclaim responsibility for any injury to people or property resulting from any ideas, methods, instructions or products referred to in the content.